2010 IEEE International Conference on Robotics and Automation
Anchorage Convention District
May 3-8, 2010, Anchorage, Alaska, USA

Wearable Cable-driven Upper Arm Exoskeleton - Motion with Transmitted Joint Force and Moment Minimization

Ying Mao and Sunil K. Agrawal
Department of Mechanical Engineering
University of Delaware
Newark, DE 19716, USA, Contact: agrawal@udel.edu

***Abstract*— Safety is a critical issue for upper arm exoskeletons intended for human use. Joint forces and moments experienced by a human user during motion must be minimized to ensure safety. Trajectory planning and control of cable-driven exoskeletons is challenging due to the unique property that cables can transmit forces only in tension. This paper introduces the design of a 4-DOF cable-driven upper arm exoskeleton and schemes for trajectory planning and control. Simulations show that in most cases a feasible point-to-point trajectory can be generated while minimizing reaction joint forces and moments.**

I. Introduction

The technology of robotic powered exoskeletons is rapidly developing today for use as assistive or rehabilitation devices. Often, these devices are made out of rigid links and have motors placed at the joints ([1], [2]), this feature makes these devices heavy and bulky. Some designs take this issue in consideration and place the motors further away from the joints ([3], [4]). This feature enhances agility. However, exoskeletons assist people with Activities of Daily Living (ADL) and this requires both agility and portability.

In recent designs, many new ideas were adopted to reduce the weight of the arm exoskeleton and enhance its agility and portability. Some designs eliminated heavy motors by using light-weight pneumatic muscles actuators ([5],[6]). This enhances agility of the robot, however, the pneumatic muscle actuators are air powered at high pressure. This limits portability of the exoskeleton. Some designs introduced light-weight cables to drive the arm exoskeletons. Typically, in these designs, the motors of the exoskeleton are placed further away from the limb and reduces extra weight of the motors on the limb ([3], [4], [7], [8], [9]). However, the rigid links are still not eliminated and this makes the exoskeleton bulky. The Cable-driven Wearable Upper Arm Exoskeleton's design at University of Delaware takes this a step further by replacing rigid link with light cables [10]. However, due to the unilateral property of cables, trajectory planning and control remains an open question. A key issue in such a design is to ensure subject safety, both at the hardware and software layers ([11], [12]). This paper addresses user safety by minimization of shoulder and elbow joint forces and moments.

II. Exoskeleton Design and Models

A. Description

The cable-driven upper arm exoskeleton consists of three aluminum cuffs that attach to the human user at the shoulder, upper arm and the forearm, as shown in Fig.1. The shoulder cuff is a semicircle that rests on the human shoulder. It has six aluminum extension pieces, each of which holds a motor. Each arm cuff has small extension pieces which serve as routing and/or attachment points for the cables. Six cables are used to drive the device, which are attached to motors on the shoulder cuff. Four of these cables are attached to the upper arm cuff and are responsible for controlling the three degrees-of-freedom at the shoulder. The other two cables are routed through the upper arm cuff to the cuff on the forearm. These cables control the elbow flexion and extension.

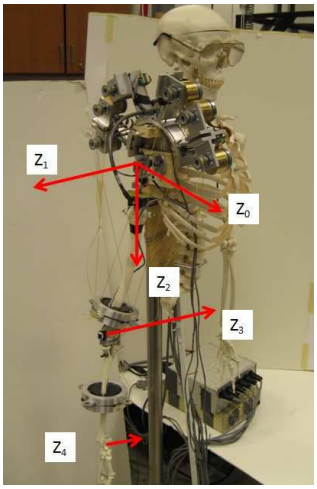

Fig. 1. A photograph of the upper arm exoskeleton mounted on an anthropomorphic arm along with joint axes.

The exoskeleton is powered by six Maxon EC 45 flat brushless motors mounted on the shoulder cuff. The motors are equipped with hall sensors that provide feedback to the motor amplifiers. Each motor is controlled by Maxon LCS 30/2 motor amplifier. The motor controller interface is via a dSpace DS1103 PPC Controller board using ControlDesk user interface.

TABLE I

D-H PARAMTERS FOR THE UPPER ARM EXOSKELETON

Link	α_i	a_i	d_i	θ_i
1	0	90	0	θ_1
2	0	90	0	θ_2
3	0	90	d_3	θ_3
4	α_4	0	0	θ_4

B. Dynamics

The dynamic equations of motion for the upper arm exoskeleton were derived in Maple using Lagrangian method. The D-H Table and joint rotation axes are shown in Table I and Fig. 1. The coordinates q_1, q_2, and q_3 represent the three degrees-of-freedom at the shoulder and q_4 denotes the elbow flexion-extension. The equations of motion have the following form:

$$D(q)\,\ddot{q} + C(q,\dot{q})\,\dot{q} + g(q) = J(q)^T T(t) \tag{1}$$

where $q = (q_1, q_2, q_3, q_4)^T$ are the generalized coordinates, $D(q)$ is the 4×4 inertia matrix, $C(q,\dot{q})$ is the vector of coriolis and centripetal terms, $g(q)$ is the vector of gravity terms, $J(q)$ is the Jacobian matrix relating cable tensions to joint moments, and $T(t)$ is the vector of cable tensions. The dynamic equations are fairly non-linear and complex, hence the detailed equations are not included in this paper but the qualitative form is only described in the paper.

A flowchart for development of the control scheme for cable robot is shown in Fig. 2. Static workspace is first optimized wherein cables can hold the system in equilibrium. A point-to-point trajectory planner ensures cables to be in tension along the trajectory and computed torque schemes are then implemented.

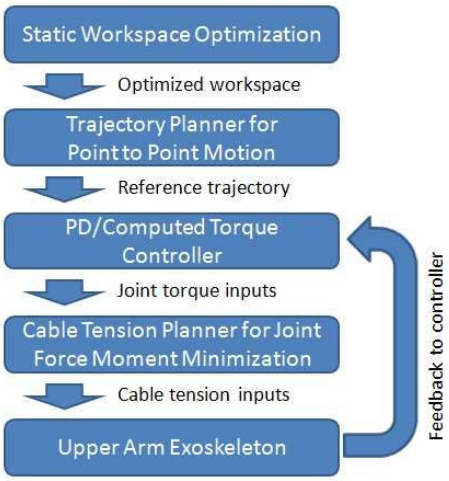

Fig. 2. The flowchart for the control scheme of the cable robot

III. TRAJECTORY PLANNER AND CONTROLLER

The cable-driven upper arm exoskeleton has been designed with the objective to help subjects in their Activities of Daily Living (ADL), e.g., move an object from place to place, operate an appliance, feed from a plate, etc. Hence, point to point motion of the hand is of great practical interest. Unlike traditional rigid link robots, cables can only drive the exoskeleton in tension. Due to this unique feature of cable-driven robots, additional thoughts are required both during trajectory planning and control.

We perform the trajectory planning in two steps: (i) Pre-planning optimization of the static workspace over the Most Frequently Used Volume (MFUV) during ADL with the arm. This static workspace is a set of points in the configuration space where the arm can be held in equilibrium with cables in tension. Optimization of this static workspace increases the chance of generating feasible trajectories within the configuration space as the exoskeletal system performs dynamic motions. (ii) Planning a trajectory between the chosen initial and final points in MFUV using a high degree polynomial in time while maximizing feasibility along the trajectory. This trajectory is used as a reference for the controller.

It is important to note that this procedure does not always guarantee a feasible trajectory. However, simulation results show that if the the two steps of optimizations are properly carried out, in most cases, the obtained trajectories are feasible and executable.

A. Computation Structure to Satisfy Tension Constraints

From the structure of Eq. (1), given $q(t)$, $\dot{q}(t)$, $\ddot{q}(t)$, the left hand side of the equation can be evaluated. In order for the motion to be feasible, one needs to find out if there exists a set of non-negative cable tensions $T(t)$ that would satisfy these equations. Mathematically, this problem can be expressed as

$$AT = B, \tag{2}$$

where $A = J(q)^T$ and B is the left hand side of Eq. (1). Here, A is a (4×6) matrix that represents four outputs and six cable inputs. This system is under-determined and the solution can be written as

$$T = \bar{A}B + N(A)\,m, \tag{3}$$

where $N(A)$ is the nullspace of A, m is a (2×1) vector of free variables that modifies the tension, and $\bar{A}$ is the minimum norm solution given by

$$\bar{A} = A^T\left(AA^T\right)^{-1}. \tag{4}$$

We construct the following optimization problem to search for a set of positive tensions that satisfies Eq. (2),

$$\begin{aligned} &\min \sum_i m_i \\ &s.t. \quad 0 \le \bar{T} + N(A)\,m \le T_{\max}, \end{aligned} \tag{5}$$

where $\bar{T} = \bar{A}B$. The goal is to minimize the sum of entries of the vector m such that each cable tension is positive and less than its maximum limit $T_{i\max}$. Optimization problem is formulated as a linear programming problem due to its computational efficiency. This construct is used extensively within workspace optimization and trajectory planning. It is important to note that the objective function could be chosen differently to achieve different goals.The objective function

in Eq.(5) is used only in workspace optimization to reduce computational intensity.

B. Optimization of Static Workspace

We define the MFUV of a human arm as the confined volume shown in Fig. 3. Points outside this region can be reached by using the hand or twisting the torso. The exoskeleton has been designed so that placement of the motor on the shoulder cuff can be changed both radially and along the circumference. Due to this feature of the cable-driven exoskeleton, one can optimize the static workspace MFUV by proper placement of the motors on the shoulder cuff[13].

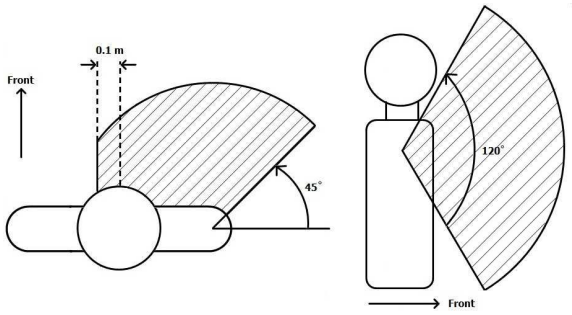

Fig. 3. Most Frequently Used Workspace(MFUV) of a human arm. Left: Overhead view. Right: Side view.

Since the optimization of feasible workspace is carried out in Cartesian space, it is also important to map this property to the joint space. As a result, inverse kinematics is required to find the joint angles for any point of the wrist in Cartesian space. There is a single infinity of joint angles that correspond to a wrist position. Hence, different choices could be made to resolve the inverse kinematics uniquely. In this paper, we choose that solution for the inverse kinematics where the plane formed by the shoulder joint, the elbow joint, and the wrist is perpendicular to the frontal plane, as shown in Fig. 4. We believe that such a configuration of the arm is naturally used in the center of the workspace of the human arm.

Since we expect the arm motion to be relatively slow, the gravity terms in Eq. (1) would dominate over the inertia and nonlinear terms. Hence, more practically, the usable workspace is the static workspace and this must be optimized by proper selection of the motor placements on the shoulder. For a given choice of motor placement parameters, the static workspace is computed by counting the total number of feasible points at which the arm can stay in equilibrium under gravity within the MFUV, i.e., when $\dot{q}$ and $\ddot{q} = 0$. This process was repeated as the angular position of the shoulder motors were varied and an optimal set was found. The elbow cable attachment points were fixed by anatomical consideration and the radial position along the shoulder cuff and upper arm cuff were chosen to simplify the number of variables in the optimization. The static workspace before and after the optimization are shown in Fig. III-B.

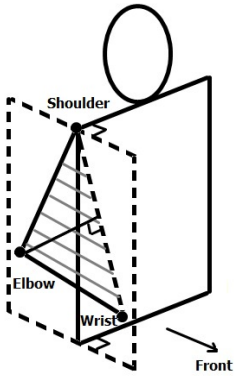

Fig. 4. Configuration selected to resolve the inverse kinematics - the plane formed by the shoulder joint, elbow joint, and the wrist is perpendicular to the frontal plane.

A total of 4292 test points are evenly distributed in polar coordinates. The feasible points increased from 2499 to 4075 after optimization.

C. Trajectory Planning for Point to Point Motion

We know that the static workspace was found such that joint speeds and accelerations are zero. In order to determine a feasible joint trajectory between two points in the joint space, a 4th-order polynomial is chosen in time for each joint variable.

$$q(t) = a_0 + a_1 t + a_2 t^2 + a_3 t^3 + a_4 t^4. \tag{6}$$

This joint trajectory has five coefficients and satisfies four initial and terminal conditions: $q(t_i) = q_i$, $\dot{q}(t_i) = \dot{q}_i$, $q(t_f) = q_f$, and $\dot{q}(t_f) = \dot{q}_f$, where t_i is the initial time and t_f is the final time. This solution form provides a free parameter to modify the trajectory in order to make it feasible. The unknowns coefficients a_0 through a_4 are found by solving the following linear equations

$$Ma = b, \tag{7}$$

where $M = \begin{bmatrix} 1 & t_i & t_i^2 & t_i^3 & t_i^4 \\ 1 & t_f & t_f^2 & t_f^3 & t_f^4 \\ 0 & 1 & 2t_i & 3t_i^2 & 4t_i^3 \\ 0 & 1 & 2t_f & 3t_f^2 & 4t_f^3 \end{bmatrix}$, $a = \begin{bmatrix} a_0 & a_1 & a_2 & a_3 & a_4 \end{bmatrix}^T$, and $b = \begin{bmatrix} q_i & q_f & \dot{q}_i & \dot{q}_f \end{bmatrix}^T$. The solution of these linear equations is given by

$$a = \bar{a} + N(M)\, k, \tag{8}$$

where $\bar{a}$ is the minimum norm solution

$$\bar{a} = M^T \left(M M^T\right)^{-1} k, \tag{9}$$

$N(M)$ is the nullspace of M and k is an arbitrary constant.

The parameter set k for the joint variables is determined by solving the following nonlinear optimization problem

$$\begin{aligned} &\min\left(n_{infeasible}\right) \\ &s.t. \quad k_{\min} \le k \le k_{\max}, \end{aligned} \tag{10}$$

where $n_{infeasible}$ is the total number of dynamically infeasible points along the trajectory, $k_{\min}$ and $k_{\max}$ are

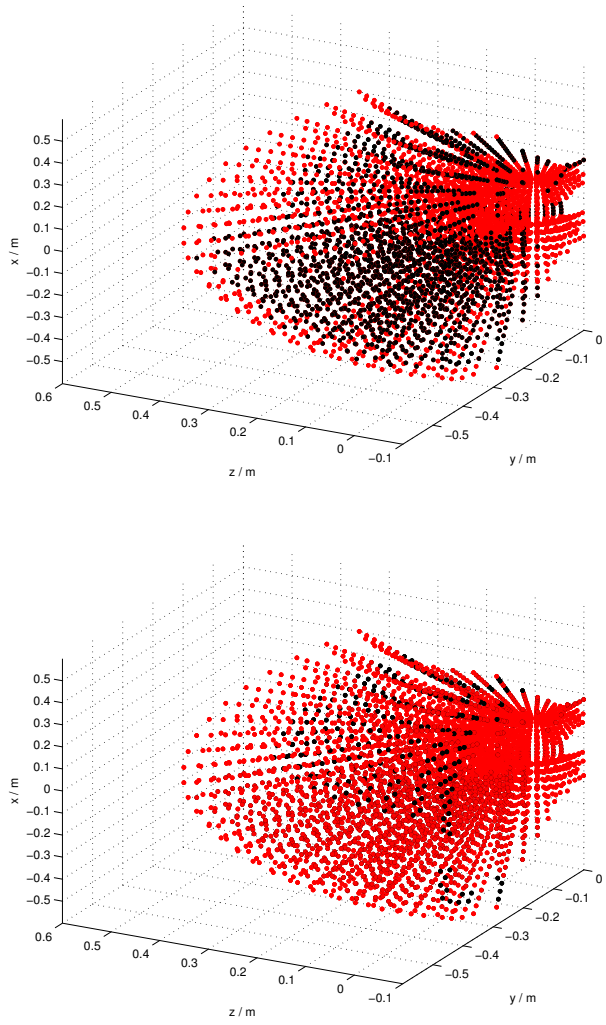

Fig. 5. Up: static workspace before optimization. Down: Static workspace after optimization. Black dots: infeasible points. Red dots: feasible points.

the lower and upper bound of decision variable k. The variable $n_{infeasible}$ is determined in two steps: (i) total time is discretized into a finite number of points, and (ii) at each time, the computational structure of Sec. III-A is used to check the infeasibility, where $q(t)$, $\dot{q}(t)$, and $\ddot{q}(t)$ are computed from Eq. (6) and substituted into Eq. (1). The results of this paper use $k_{\min}$ and $k_{\max}$ as -400 and 400, respectively and the total number of evenly spaced points in time are 200.

D. Feedback Controllers

The following feedback control structures can be used: (i) PD controller with gravity balancing, (ii) Computed torque controller:

$$u = K_p\left(q_d - q\right) - K_d\dot{q} + g\left(q\right), \qquad u = D\left(q\right)\left(\ddot{q}_d - K_d\dot{e} - K_p e\right) + C\left(q,\dot{q}\right)\dot{q} + g\left(q\right) \quad (11)$$

where $e = q - q_d$. K_p and K_d are proportional and derivative gains, respectively. q_d is the desired joint angle updated according to pre-planned trajectory.

IV. Minimizing Transmitted Reaction Force and Moments

With the intended use of this device by humans, safety is of paramount importance. The forces transmitted to the shoulder are two-fold: (i) Reaction forces and moments at the shoulder joint, (ii) Since the shoulder cuff is mounted directly on the human shoulder, the tensions applied on the cables by the motors are transmitted to the shoulder due to action-reaction principle. From the perspective of safety, we evaluate the reaction force and moment at the shoulder joint and present a scheme of how to execute trajectories to keep these within safety limits.

A. Computation of Joint Forces and Moments

The free body diagram for the upper arm and the forearm are shown in Figs. 6 and 7, respectively. Free-body analysis

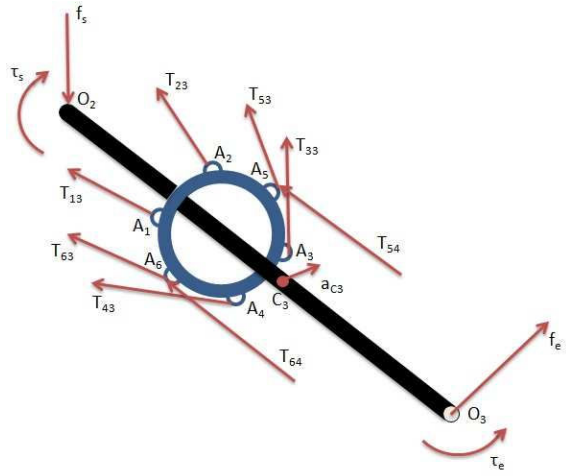

Fig. 6. Freebody diagram of the upper arm (body 3)

gives the following Newton-Euler equations for the upper and the fore arms

$$\begin{aligned}
&m_4\vec{a}_{C_4} = -\vec{f}_e + \vec{T}_{54} + \vec{T}_{64} + m_4\vec{g}\\
&I_4\cdot\dot{\vec{\omega}}_4 + \vec{\omega}_4\times I_4\cdot\vec{\omega}_4 = -\vec{\tau}_e - \vec{r}_{C_4O_3}\times\vec{f}_e\\
&\qquad + \vec{r}_{C_4E_5}\times\vec{T}_{54} + \vec{r}_{C_4E_6}\times\vec{T}_{64}\\
&m_3\vec{a}_{C_3} = -\vec{f}_s + \vec{f}_e + \vec{T}_{13} + \vec{T}_{23} + \vec{T}_{33}\\
&\qquad + \vec{T}_{43} + (\vec{T}_{53} - \vec{T}_{54}) + (\vec{T}_{63} - \vec{T}_{64}) + m_3\vec{g}\\
&I_3\cdot\dot{\vec{\omega}}_3 + \vec{\omega}_3\times I_3\cdot\vec{\omega}_3 = -\vec{\tau}_s + \vec{\tau}_e + \vec{r}_{C_3O_3}\times\vec{f}_e\\
&\qquad - \vec{r}_{C_3O_2}\times\vec{f}_s + \vec{r}_{C_3A_1}\times\vec{T}_{13} + \vec{r}_{C_3A_2}\times\vec{T}_{23}\\
&\qquad + \vec{r}_{C_3A_3}\times\vec{T}_{33} + \vec{r}_{C_3A_4}\times\vec{T}_{43}\\
&\qquad + \vec{r_{C_3A_5}}\times(\vec{T}_{53} - \vec{T}_{54}) + \vec{r}_{C_3A_6}\times(\vec{T}_{63} - \vec{T}_{64}),
\end{aligned} \quad (12)$$

where the nomenclature is provided in Table II.

All matrices and vectors are expressed in the inertial frame fixed to the shoulder. All quantities in Eq. (12) are known or can be computed from joint angles $q(t)$ and their derivatives, except for f_e, τ_e, f_s and τ_s. Therefore, once the tensions $T(t)$

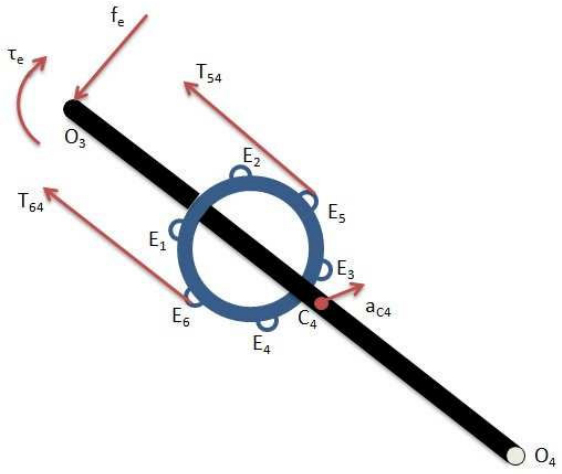

Fig. 7. Freebody diagram of the forearm (body 4). **Note negative signs on reaction force/moment**

TABLE II

NOMENCLATURE FOR VARIABLES IN FREE-BODY DIAGRAMS

Notation	Definition
m_i	Mass of body i.
I_i	Inertia matrix of body i.
$\vec{g}$	Gravity.
$\vec{a}_{C_i}$	Acceleration of center of mass of body i.
$\vec{\omega}_i$	Angular acceleration of body i.
$\vec{T}_{ij}$	Tension acting on body$j$ by cable i.
$\vec{f}_s/\vec{f}_e$	Reaction force at shoulder/elbow.
$\vec{\tau}_s/\vec{\tau}_e$	Reaction moment at shoulder/elbow.
$\vec{A}_i$	Attaching position of the ith cable on the mid-upper arm cuff.
$\vec{E}_i$	Attaching position of the ith cable on the mid-fore arm cuff.
$\vec{R}_{X_iY_i}$	Vector from $\vec{X}_i$ to $\vec{Y}_i$.

in the cables and the joint angle $q(t)$ are known, joint forces f_e, f_s and moments τ_e,τ_s can be found by solving Eq. (12).

B. Tensions to maximize Human safety

The computation structure of Section III-A is used to perform this step. We define safety indices, which are ratios between actual force/moment and the minimum force/moment that would injure a human at shoulder and elbow joints [14]. We seek to minimize the maximum safety index among R_{fe}, $R_{\tau e}$, R_{fs}, $R_{\tau s}$, where f denotes force, τ the moment, e for elbow and s for shoulder. The optimization problem is written as

$$\begin{aligned} &\min \{\max (R_{fe}, R_{\tau e}, R_{fs}, R_{\tau s})\} \\ s.t. \quad &0 \leq \bar{T} + N(A) \cdot m \leq T_{\max} \end{aligned} \tag{13}$$

The safety indices are functions of cable tension T, therefore, functions of decision variable m. This optimization problem is nonlinear and becomes computational intensive.

V. SIMULATION

We performed several simulations to validate the planners and controllers presented in the previous sections. In the simulations, parameters such as lengths and masses weere measured from the experiment device except for the rotational inertias of different bodies which were estimated. After static workspace optimization, we chose $x_i = [-0.4731, -0.1698, 0.2536]$ and $x_f = [-0.4321, -0.2044, 0.3156]$ as the initial and final points. A feasible trajectory was planned between these end points. We introduced a small error at the initial point and used both Trajectory tracking PD controller and Trajectory tracking computed torque controller to move the hand from $x_i' = [-0.4684, -0.1757, 0.2612]$ to x_f. The results are shown in Fig. 8. We observe that both controllers successfully accomplish the task, as expected. The two controllers did not have significant differences in tracking performance, though computed torque controller reached the steady-state slightly faster than PD controller.

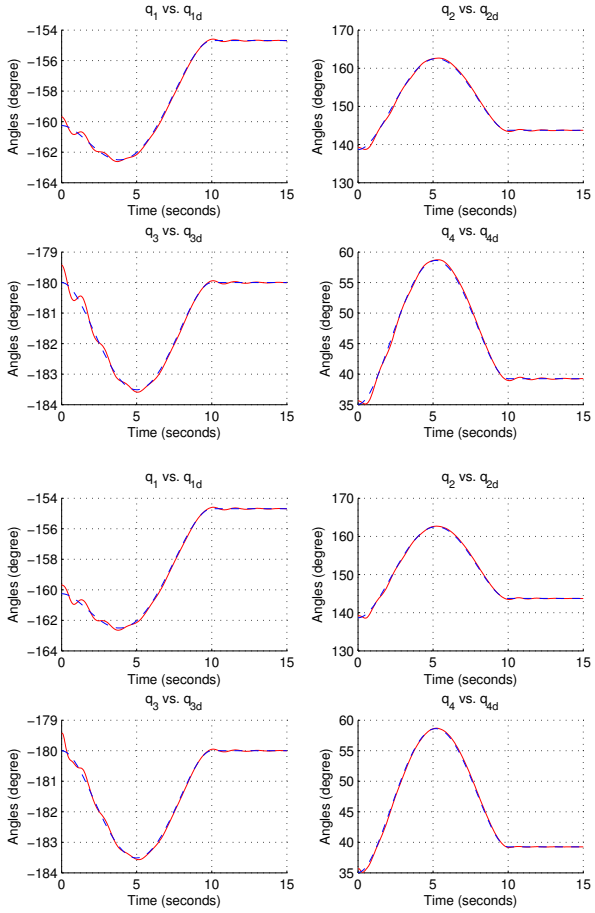

Fig. 8. Left: Trajectory tracking using PD controller. Down: Trajectory tracking using Computed-Torque controller. Blue dashed line: Reference Trajectory. Red solid: Actual Trajectory

The joint force and moment were computed for the same motion without and with the force/moment minimizing cable tensions. In these simulations, the same computed torque controller was used. The minimal impact force/moment were estimated as $f_{e\,critical} = 20N$, $f_{s\,critical} = 100N$, $\tau_{e\,critical} = 1N \cdot m$, and $\tau_{s\,critical} = 4N \cdot m$. Simulation results are shown in Fig.9. We notice a 10% to 50% decrease of shoulder joint reaction force and moderate change in

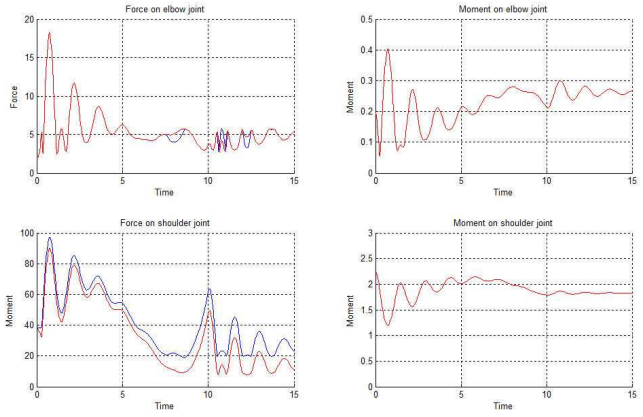

Fig. 9. Blue: Joint forces and moments without force/moment minimizing cable tensions. Red: Joint forces and moments with force/moment minimizing cable tensions

elbow joint force. The elbow and shoulder moments remain almost unchanged. This is because most of the time during motion, the safety index of shoulder joint force is the largest and was minimized.

In order to validate the computation of joint force and moment, we also computed the joint moment component along the axis of rotation of the elbow and shoulder. These components should be zero at all times. We see in Fig. 10 that during the motion, these components were always zero validating our computations.

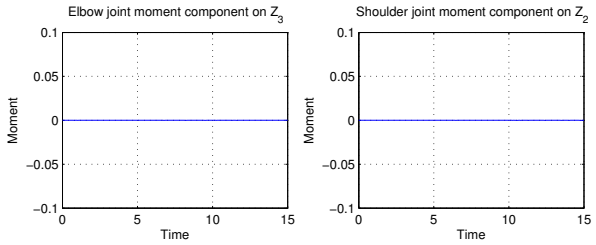

Fig. 10. Joint moment components along axes of rotation of elbow and shoulder.

Many simulations were carried out with different initial and finial points. Similar results were obtained in most cases, however, we did have difficultly generating feasible trajectories for some combinations of initial and final points. Most of these could be fixed if the initial point or the final points were altered mildly.

VI. Conclusion and Future Work

It was shown that static workspace optimization and trajectory planning allowed us to carry out point to point motion with the upper-arm exoskeleton, despite unilateral constraints of the cables. Simple PD controllers or computed torque controllers could be used to correct for initial errors. Though this process does not guarantee motion always, it was found in simulation that in most cases a feasible path could be generated and point to point motion could be achieved. However, the comfort of the generated trajectory for human subjects needs to be further investigated in the future. It was also shown that the cable tension planner makes it possible to minimize the joint forces and moments, which is of critical importance for safety. However this current algorithm is formulated as a nonlinear optimization problem. In the near future, this algorithm will be modified to include ideas from receding horizon control from the perspective of real-time implementations.

A new experiment set up, addressing better motor control capabilities and exoskeleton wearability, is currently under construction at Mechanical System Laboratory at University of Delaware. Experiments validating the optimization and planning discussed in previous sections will be carried out in the near future.

References

[1] A. Gupta and M. K. O'Malley, "Design of a haptic arm exoskeleton for training and rehabilitation," *Mechatronics, IEEE/ASME Transactions on*, vol. 11, pp. 280–289, 2005.

[2] C. Carignan, M. Liszka, and S. Roderick, "Design of an arm exoskeleton with scapula motion for shoulder rehabilitation," *Advanced Robotics, 2005. ICAR '05. Proceedings. , 12th International Conference on*, pp. 524–531, 2005.

[3] J. C. Perry, J. Rosen, and S. Burns, "Upper-limb powered exoskeleton design," *Mechatronics, IEEE/ASME Transactions on*, vol. 12, 2007.

[4] K. Kiguchi and et al., "Development of a 3dof mobile exoskeleton robot for human upper-limb motion assist," *Robotics and Autonomous Systems*, vol. 56, 2008.

[5] N. Tsagarakis and D. Caldwell, "Development and control of a soft-actuated exoskeleton for use in physiotherapy and training," *Autonomous Robots*, vol. 15, 2003.

[6] S. Balasubramanian, R. Wei, M. Perez, B. Shepard, E. Koeneman, J. Koeneman, and J. He, "Rupert: An exoskeleton robot for assisting rehabilitation of arm functions," *2008 Virtual Rehabilitation, IWVR*, pp. 163–167, 2008.

[7] G. Yang, M. S. Kurbanhusen, C. B. Pham, and S. H. Yeo, "Kinematic design of a 7-dof cable-driven humanoid arm:a solution-in-nature approach," *Advanced Intelligent Mechatronics, Proceedings of the 2005 IEEE/ASME International Conference on*, pp. 444–449, 2005.

[8] S. Ball, I. Brown, and S. Scott, "A planar 3dof robotic exoskeleton for rehabilitation and assessment," *29th Annual International Conference of IEEE-EMBS, Engineering in Medicine and Biology Society*, pp. 4024–4027, 2007.

[9] F. Martinez, I. Retolaza, A. Pujana-Arrese, A. Cenitagoya, J. Basurko, and J. Landaluze, "Design of a five actuated dof upper limb exoskeleton oriented to workplace help," *Proceedings of the 2nd Biennial IEEE/RAS-EMBS International Conference on Biomedical Robotics and Biomechatronics, BioRob 2008*, pp. 169–174, 2008.

[10] E. Brackbill, Y. Mao, S. Agrawal, M. Annapragada, and V. Dubey, "Dynamics and control of a 4-dof wearable cable-driven upper arm exoskeleton," *Robotics and Automation, 2009 IEEE International Conference on*, pp. 2300–2305, 2009.

[11] R. Gopura and K. Kiguchi, "Distributed control and safety system for a rehabilitation arm exoskeleton," *ASME International Mechanical Engineering Congress and Exposition, Proceedings*, pp. 1325–1334, 2008.

[12] S. Roderick and C. Carignan, "An approach to designing software safety systems for rehabilitation robots," *Proceedings of the 2005 IEEE 9th International Conference on Rehabilitation Robotics*, pp. 252– 257, 2005.

[13] S. Agrawal, V. Dubey, J. Gangloff, E. Brackbill, Y. Mao, and V. Sangwan, "Design and optimization of a cable driven upper arm exoskeleton," *Journal of Medical Device*, vol. 3, 2009.

[14] K. Ikuta, H. Ishii, and M. Nokata, "Safety evaluation method of design and control for human-care robots," *The International Journal of Robotics Research*, vol. 22, 2003.